The effects of exhaust gas recirculation on NO_x storage pathway

Jin Zhao[1,*], *Zhijun* Li[1], *Shilong* Li[1], *Shijin* Shuai[2], *Shiyu* Liu[2], and *Lijuan* Cao[3]

[1] State Key Laboratory of Engines, Tianjin University, Tianjin 300072, China
[2] State Key Laboratory of Automotive Safety and Energy, Tsinghua University, Beijing 100084, China
[3] China Automotive Technology & Research Center Co. Ltd, Tianjin 300300, China)

Keywords: Lean NO_x Trap, EGR, nitare route, nitrite route, NO_x srotage.

Abstract. A LNT (lean NO_x trap) model coupled with EGR (exhaust gas recirculation) was developed based on the Langmuir–Hinshelwood mechanism to investigate the EGR effects on NO_x adsorption pathway of LNT catalysts with temperature changed in range 150℃~550℃. Both the nitrate and nitrite adsorption paths were considered for the NO_x storage process in the model as well as the spillover of stored NO_x between Ba and Pt sites. The data and validation for modelling were from literatures of predecessors and our previous lean-burn gasoline engine experiment[*]. The model quantified the contributions of both nitrate route and nitrite route to the NO_x storage with change of EGR rate (0%~30%) under raw emission atmosphere from tested gasoline engine. The model captured key feature of different trends of nitrate route and nitrite route with increasing temperature (150℃~550℃) under EGR rate varying from 0% to 25%. The LNT model provided insight of reaction mechanism for interpreting the behaviour of NO_x storage with change of GER rate and temperature, which contributed to improve the NO_x storage capacity when mapping EGR rate for lean-burn engine and catalyst operation strategy optimization.

Highlights

- Nitrate route and nitrite route had complementary correlation with each other
- There were opposite effects of EGR on two NO_x storage routes in low EGR rate range
- Ratio of nitrate route to nitrite route was lowest at moderate EGR rate
- Ratio of two routes was mainly decided by nitrite route at low and high temperature
- The degree to which EGR affected the two routes varied with EGR rate and temperature

[*] Corresponding author: 18169545907@163.com

1 Introduction

Lean NO_x Trap also known as NSR (NO_x storage and reduction) is one of effective ways to reduce NO_x emission of diesel and lean-burn engines with good fuel economy[1]. The common LNT consisted of a noble metal (PGM specially Pt as catalyst sites for NO_x oxidation and reduction) plus alkaline or alkaline-earth compounds (mostly Ba as NO_x storage sites) deposited on alumina over a monolithic structure, usually cordierite[2]. NO_x adsorption and reduction are based on cyclical engine operation alternating between lean-burn (lean fuel, high air-to-fuel ratio A/F) and rich-burn (fuel rich, A/F<13.63/1 w/w) modes[3]. NO_x is adsorbed on the catalyst surface by alkali or alkaline-earth oxides under lean-burn environment, while the adsorbed NO_x is reduced during rich-burn phase to regenerate catalyst[4][5].

Generally summarize literatus of LNT or NSR, there are five following steps to reveal the NO_x storage and reduction mechanisms[6][7]: 1.NO Oxidation during lean conditions; 2. NO_x adsorption on storage sites as nitrites and nitrates; 3. reductant agent evolution and by-products reaction; 4. stored NO_x release from catalyst surface to gas flow; 5. Reduction of gaseous NO_x or stored NO_x to N_2 during the rich environment. The work about NO_x adsorption process is a focus among recent LNT researches. Basically, NO_x adsorption in LNT can be summarized as two parallel pathways. NO is oxidized to NO_2 with precious metal catalyzing firstly, and subsequently adsorbed on NO_x storage sites as nitrates involving the disproportionation reaction of NO_x and formation of barium peroxide and so on, which was noted as nitrate route[8]. Another path is nitrite route, i.e., NO can be stored directly in the presence of NO and oxygen as nitrite species, then further oxidized to stable nitrates by O_2 and NO_2 from both gas phase and surface sites[9].

Lots of researches were done to study the difference between two pathway and respective contribution to NO_x storage performance, at same boundary conditions such as inlet gas components and temperature which have a great influence on both NO_x storage pathways. Morandi S et al.[10] pointed out that the nitrites possess is significantly lower stability due to thermal stability of the nitrates is significantly higher. Nova et al.[11] and Lietti et al.[8] demonstrated that the NO_x disproportionation reaction did not represent the major storage route under NO and NO/O_2 mixtures due to the presence of nitrites in higher amounts than nitrates during the initial NO_x adsorption at low temperatures. Same conclusion can be seen in Castoldi L et al.[12] works which have confirmed participation of nitrite at 150℃, and nitrite only can be observed at the beginning of adsorption phase at 350℃. Epling W S et al.[13] revealed that the two of major components of lean-burn engine exhaust, CO_2 and H_2O, compete for the same NO_x adsorption sites, resulting in reduction of NO_x storage capacity of LNT. Lindholm A et al.[14] through the study, Influence of H_2O and CO_2 on NO_x storage and reduction over Pt based catalysts with hydrogen as the reducing agent, has shown that H_2O and CO_2 of the inlet stream lead to the formation of hydroxide and carbonate species on adsorption sites. The hydroxide and carbonate species associated with the alkaline or alkaline-earth adsorption sites reduced the trapping efficiency of NO_x, because it's more difficult to store NO_x on $Ba(OH)_2$ and $BaCO_3$ than on BaO. Furthermore, Epling W S et al.[13] found that hydroxide species formed by H_2O with Ba sites could be displaced by carbonate species due to its higher stability. It should be aware of that oxidation of NO to NO_2 is a key initial step before NO_x storage on alkaline or alkaline-earth component because NSR catalyst is more efficient to sorb NO_2 compared with NO on the NO_x storage sites. Auvray X P, Olsson L et al.[15] studied the inhibition effects of H_2O on NO oxidation, pointed out that Pt sites are blocked by water adsorbed on it at low temperature for oxygen adsorption on Pt surface. Whereas Ren Y, Harold M P et al.[16] demonstrated that NO_x storage or global NO_x convection were almost impervious to H_2O effects on NO oxidation.

The nitrites on certain temperature range are discussed in reference [17] and [10], and CO_2 has inhibition effect on adsorption, H_2O has little influence on both adsorption paths.

EGR is an effective way to reduce engine NO_x emissions. F. Sarikoc, M. Kettner et al.[18] research studied the potential of reducing the NO_x emissions in a spray guided DI gasoline engine by stratified exhaust gas recirculation (EGR). Lapuerta, M. et al.[19] research showed that low-pressure exhaust gas recirculation was more efficient than high-pressure exhaust gas recirculation to reduce NO_x emissions, mainly due to the higher recirculation potential and the lower temperature of the recirculated gas. However, such a differential benefit decreased as the coolant temperature decreased, which suggests the use of high-pressure exhaust gas recirculation during the engine warm-up. It was also shown that the lean-NO_x trap storage efficiency decreased more rapidly at high engine load than at medium load and that such reduction in efficiency was much faster when high-pressure exhaust gas recirculation was used than when low-pressure exhaust gas recirculation was used. Previous researches of our group were about influence of the coupling of EGR and lean-burn gasoline engine with the LNT catalyst[20]. We pointed out that the main reason of the EGR effects on LNT overall performance was the inlet components CO_2\H_2O concentration and ratio changed with EGR rate.

There are few researches combining CO_2 and H_2O to the overall level of EGR to study detailed mechanism of its effects on LNT catalyst specific work stage such as NO_x storage step under raw emission atmosphere from tested gasoline engine, though lots of researches done to study the effects of inlet components CO_2\H_2O on NO oxidation, NO_x trap efficiency and NO_x convection. In addition, our preliminary experimental researches focused on the discovery of the phenomenon and overall performance of synergetic system of coupling EGR with LNT, which did not conduct deep research on the influence of EGR on LNT and the underlying detailed mechanism. Hence, a detailed lean NO_x trap (LNT) adsorption model coupled with EGR was developed based on the Langmuir–Hinshelwood mechanism, and both the nitrate and nitrite adsorption pathways were considered in the model as well as the NO_x spillover steps between Ba\Pt sites. In additional, raw emission compositions were as boundary conditions for the LNT-EGR model.

2 Experiment setup

Figure 1 showed the layout of lean-burn gasoline engine test bench with EGR and LNT after-treatment system. A commercial LNT catalytic converter (Pt/Ba/Al2O3) made by Toyota with the volume of 1.9 L was chosen for simulation and experiment. The rate of exhaust flow was 950 L/min, and tested initial exhaust temperature was set as 350℃ which was favorable for high NO_x conversion. The fixed inlet temperature of LNT can be controlled by the device 20 showed in Figure 1. The ratio of lean-burn time to rich-burn time was set as 56 s : 7 s in consideration of the balance the NO_x storage capacity and slip of NO_x during the switch of lean-rich condition, i.e., NO_x storage sites were not saturated within the adsorption time 56s for the sake of reducing NO_x release and maintaining overall NO_x conversion efficiency. The AFR (Air/Fuel ratio) during lean-burn phase was 23, while the AFR for rich condition was 12.

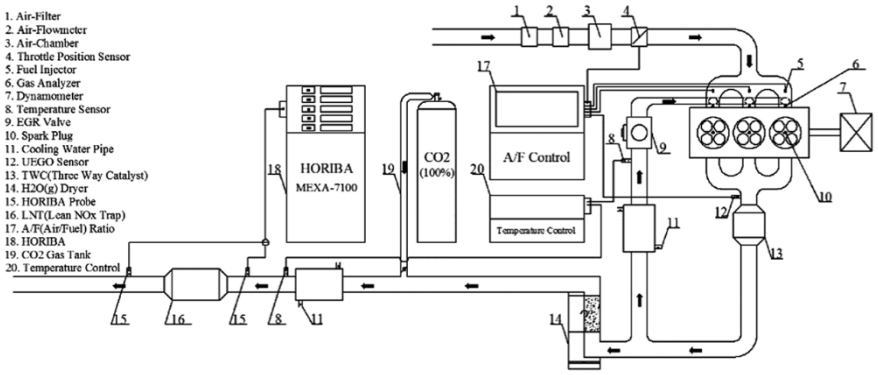

Fig. 1. Layout of lean-burn gasoline engine test bench with EGR and LNT after-treatment system.

Table 1. The main characteristic parameters of LNT catalyst.

LNT Characteristic Parameters	Numerical value
Catalyst	$Pt/BaO/Al_2O_3$
Pt Loading (g/ft^3)	50
Active metal surface (m^2/g)	28
Pt dispersion (%)	25
Surface site density S_{DEN} of Pt (mol/cm^2)	8.095E-08
Surface site density S_{DEN} of Ba(mol/cm^2)	8.846E-07
Catalyst volume(L)	1.9
Carrier length(mm)	200
Carrier diameter(mm)	110
Catalyst length(mm)	480
Catalyst inlet diameter(mm)	50
Diffusion/shrink length(mm)	40
CPSI(Cells Per Square Inch)	400

Table 1 listed the LNT characterization paramaters, and measured raw emissions of engine under different EGR rate which were used as inlet conditions for the LNT-EGR model were shown in Table 2, the more details about the bench experiment can be found in our previous paper.[20]

Table 2. Measured inlet gas composition and concentration of LNT with different EGR rate.

EGR	HC/ppm(ppm)	CO/ppm(ppm)	CO_2/ppm(ppm)	NO/ppm(ppm)	NO_2/ppm(ppm)	O_2/ppm(ppm)	H_2O/ppm(ppm)
0%	58.90	14.05	106000	1090	109	68400	34328
	3590	30180	110000	27.6	2.76	27400	38799
10%	63.9	15.35	119000	1000	100	64500	25320
	3610	35200	123000	24.4	2.44	23500	24663
15%	68.9	15.85	125000	882.7	88.27	60600	23344
	3670	40200	129000	22.4	2.24	19600	17505
20%	73.9	16.13	127800	414.6	41.5	56800	24853
	3720	45200	131800	20	2	15800	13458
25%	78.9	16.63	136300	391	39.9	52000	21174
	3770	50200	140600	17.8	1.78	13000	2410

30	83.9	17.13	146100	375	37.5	48000	15386
%	3820	55200	150600	17.2	1.72	11000	1000

Noting that there were two rows data of inlet gas composition and concentration corresponded to each EGR rate in the first column on left side, the data of above row referred to lean conditions of inlet gas composition, while the below row was belonging to rich condition. (The rest inlet gas is N_2 by default)

3 Modelling

3.1 Reactor model

The Perfectly Stirred Reactor (PSR) model is a reaction model in the CHEMKIN software to simulate the process and mechanism of NOx storage and reduction in LNTs. It is a coupled system consisting of gas phase chemical reactions and surface chemical reactions, in which chemical kinetic processes play a leading role. There are assumptions and limitations, first the mass transport from bulk gas to surface (channel wall) was infinitely fast, and the relative importance of the reaction depends only on the specific surface area of the substance. Second, the flow through reactor is characterized by a nominal residence time, which can be deduced from the flow rate and the reactor volume. Based on the above assumptions, the equations used in the PSR reactor model are listed below.

Global mass conservation in the reactor volume

$$\frac{\mathrm{d}}{\mathrm{d}t}(\rho V) = \dot{m}^* - \dot{m} + \sum_{m=1}^{M} A_m \sum_{k=1}^{K} \dot{s}_{k,m} W_k \tag{1}$$

Left side of the Equation 1 is the time-rate of change of the mass in the reactor, and the right side is the difference between the mass flow in and the mass flow out, plus the net production of species on the surface material. ρ is the mass density of a gas mixture (g/cm^3), V is control volume (cm^3), $\dot{m}^*$ is the inlet mass flow rate (g/sec), $\dot{m}$ is the outlet mass flow rate (g/sec). A_m is the surface area of the material m defined within the reactor (cm^2). $\dot{s}_{k,m}$ is the molar surface production rate of the species k on the material m per unit surface area (mole/(cm^2/sec)). W_k is molecular weight of the species k. K and M represent the total gas-phase species and materials, respectively.

Surface species conservation equation

$$\frac{\mathrm{d}}{\mathrm{d}t}(A_m c_k W_k) = A_m \dot{s}_{k,m} W_k \tag{2}$$

Here A_m is the surface area of the material m in the reactor and c_k is the molar concentration of the surface species k (mole/cm^2).

The model introduced in this article is an ideal PSR reaction model. Since catalysis only reacts on the surface, there is no gas phase reaction, so the energy equation of the gas phase reaction is not discussed here.

3.2 Reaction mechanism

Based on the CHEMKIN which is the standard for modeling and simulating gas-phase and surface chemistry through specific development, the gas phase, surface phase and thermodynamics files developed by data from experiments and simulations of predecessors and our previous lean-burn gasoline engine experiment were rewritten for the NO_x adsorption process of the LNT-EGR model. A modification LNT model based on Chatterjee D et al.[21][22][23] research was built. The detailed reactions involved in the mechanism and the

related chemical kinetic parameters were shown in Table 3, which described NO_x storage and reduction under isothermal conditions.

Table 3. Reaction scheme of LNT and the parameter value of Arrhenius rate expression.

	reaction	A_i		β_i		E_i (cal/mole)	
		forward reaction	reverse reaction	forward reaction	reverse reaction	forward reaction	reverse reaction
	Surface mechanism on Pt						
R1	NO + Pt(S) ↔ NO(S)	3.890E+13	5.818E+12	0	0	25.79	72.82
R2	NO_2 + Pt(S) ↔ NO_2(S)	2.248E+10	1.961E+14	0	0	17.97	100.51
R3	CO + Pt(S) ↔ CO(S)	2.594E+21	1.130E+14	0	0	99.99	99.99
R4	H_2O + Pt(S) ↔ H_2O(S)	5.071E+13	2.992E+12	0	0	53.83	87.07
R5	NH_3 + Pt(S) ↔ NH_3(S)	7.574E+30	1.329E+27	0	0	193.14	193.44
R6	O_2 + 2Pt(S) ↔ 2O(S)	4.776E+24	2.070E+29	0	0	58.39	182.81
R7	H_2 + 2Pt(S) ↔ 2H(S)	1.058E+23	8.436E+21	0	0	51.93	81.06
R8	CO(S) + O(S) ↔ CO_2 + 2Pt(S)	1.073E+13	4.783E+21	0	-0.4874	7.54	228.90
R9	2N(S) ↔ N_2 + 2Pt(S)	2.773E+16	3.587E+11	0	0.0482	88.13	123.47
R10	NO(S) + NH(S) ↔ N_2O(S) + H(S)	9.373E+11	2.270E+20	0.6092	0	45.87	41.70
R11	2N(S) + O(S) ↔ N_2O(S) + 2Pt(S)	2.102E+32	1.524E+29	0	-0.6092	164.37	56.44
R12	NO(S) + Pt(S) ↔ N(S) + O(S)	9.392E+18	1.383E+25	0	0	85.01	174.58
R13	NO(S) + O(S) ↔ NO_2(S) + Pt(S)	4.862E+25	1.868E+30	0.2231	0	168.59	200.69
R14	H(S) + OH(S) ↔ H_2O(S) + Pt(S)	1.945E+20	6.140E+25	0	0.6230	0.82	160.82
R15	H(S) + O(S) ↔ OH(S) + Pt(S)	2.348E+21	3.379E+11	0	0	0.00	21.03
R16	NH_3(S) + Pt(S) ↔ NH_2(S) + H(S)	6.057E+18	3.619E+28	0.8602	0	105.34	142.89
R17	NH(S) + H(S) ↔NH_2(S) + Pt(S)	1.179E+12	4.772E+20	0	0	19.12	87.26
R18	N(S) + H(S) ↔ NH(S) + Pt(S)	9.604E+22	4.234E+17	0	0	89.08	74.89
R19	NH_3(S) + O(S) ↔ NH_2(S) + OH(S)	3.367E+18	2.895E+18	0	-0.8602	33.26	91.85
R20	NO(S) + H(S) ↔ N(S) + OH(S)	3.563E+11	.548E+07	0	0	17.43	128.03
R21	N_2O(S) + H(S) ↔ N_2+OH(S) + Pt(S)	1.976E+28	5.073E+16	0	0.6574	105.34	269.64
R22	2NO(S) ↔ N_2O(S) + O(S)	7.201E+20	1.132E+30	0	-0.6092	86.38	157.59
R23	NO_2(S) + CO(S) ↔ NO(S) + CO_2 + Pt(S)	5.620E+20	6.518E+24	0	-0.2643	87.77	277.03
R24	H_2O(S) + CO(S) ↔ 2H(S) + CO_2	6.396E+18	6.274E+31	0	-1.1104	108.42	148.75
R25	N(S) + CO ↔ NCO(S)	2.879E+19	7.933E+13	0	0	106.46	118.75
R26	NCO(S) + H_2O(S) ↔ NH_2(S) + CO_2 + Pt(S)	7.648E+20	2.116E+35	0	-1.1104	96.32	178.31
R27	N_2O + Pt(S) ↔ N_2O(S)	1.976E+11	7.936E+11	0	0	35.90	35.90
R28	NO(S) + NH_2(S) ↔ N_2 + H_2O(S) + Pt(S)	1.492E+09	7.240E+02	0	0.6712	6.87	258.86

	Reactions on NO_x storage (BaO) sites						
	BaO-CO2-NO2 Surface mechanism on Pt						
R29	$CO_2 + BaO \leftrightarrow BaCO_3$	3.589E+07	1.307E+03	0	0	20.13	37.64
R30	$NO_2 + BaO \leftrightarrow BaO(NO_2)$	1.107E+08	1.292E+01	0	0	0.00	28.55
R31	$BaO + NO_2 \leftrightarrow BaO(O) + NO$	1.188E+08	8.343E+11	0	0.2231	3.93	33.14
R32	$NO_2 + BaO(NO_2) \leftrightarrow NO + BaO(NO_3)$	2.518E+08	6.599E+11	0	0	1.15	30.71
R33	$NO_2 + BaO(NO_3) \leftrightarrow Ba(NO_3)_2$	5.896E+07	7.727E+00	0	0	7.29	35.93
	Pt-BaO Spillover reactions						
R34	$BaO + O(S) \leftrightarrow BaO(O) + Pt(S)$	3.577E+13	1.655E+17	0	0	74.88	98.88
R35	$BaO(NO_2) + O(S) \leftrightarrow BaO(NO_3) + Pt(S)$	2.402E+04	4.145E+07	0	-0.2231	0.00	24.35
R36	$BaO(NO_2) + H(S) \leftrightarrow BaO + NO + OH(S)$	4.538E+08	8.496E+05	0	0.2231	2.31	0..00
R37	$Ba(NO_3)_2 + H(S) \leftrightarrow BaO(NO_2) + NO_2 + OH(S)$	7.627E+10	4.852E+04	0	0.2231	42.01	10.05
R38	$BaO(NO_2) + CO(S) \leftrightarrow BaO + NO + CO_2 + Pt(S)$	8.718E+12	5.055E+28	0	-0.2643	57.36	255.38
R39	$BaO(NO_3) + CO(S) \leftrightarrow BaO(NO_2) + CO_2 + Pt(S)$	6.517E+06	1.683E+12	0	-0.2643	0.48	197.49
R40	$Ba(NO_3)_2 + CO(S) \leftrightarrow BaO(NO_2) + NO_2 + CO_2 + Pt(S)$	4.423E+07	8.714E+19	0	-0.2643	19.14	187.51
R41	$BaO(NO_2) + N(S) \leftrightarrow BaO(O) + N_2O(S)$	1.498E+11	1.439E+24	0	-0.3861	55.14	82.67
R42	$BaO(NO_2) + N(S) \leftrightarrow BaO(O) + N_2 + O(S)$	3.535E+15	6.058E+26	0	0.2713	98.45	269.25
R43	$BaO(NO_3) + N(S) \leftrightarrow BaO(O) + N_2 + O_2 + Pt(S)$	1.216E+17	2.786E+20	0	0.4944	106.20	128.23
R44	$Ba(NO_3)_2 + N(S) \leftrightarrow BaO(NO_3) + N_2 + O_2 + Pt(S)$	1.396E+21	1.063E+24	0	0.2713	156.02	178.31

Noting that (s) behind a specie means that Pt sites were occupied by the specie, specially Pt = Pt(s).

The kinetics model includes two kinds of NO_x adsorption routes. The global reactions of nitrate route are shown in Equations 3, which consists of two types reaction path including NO_x disproportionation (Equation 3.1 & Equation 3.2) and reaction involving the formation of barium peroxide (Equation 3.3 & Equation 3.4)[24]. NO_x disproportionation (Equation 3.1 & Equation 3.2) involving nitrite and nitrate intermediates $Ba(NO_2)(NO_3)$ (refer to as $BaO(NO_2)$ & $BaO(NO_3)$ of Table 3) in reaction R30, R32 and R33) are obtained by combining R30, R32 and R33. Then, nitrites are oxidized by NO_2 in a reaction where nitrates are formed, and NO is desorbed into the gas phase[24]. As we can see from the disproportionation reaction, consumption of every three molecules of NO_2 released one molecule of NO. As for Equations 3.3 & 3.4 involving the formation of barium peroxide and NO are the global reactions of reactions R31, R6, R9, R12, R13, R43 and R44. Barium surface can be oxidized by NO_2 involving the formation of barium peroxide and NO which

is released in the gas phase[24]. Then BaO(O) is involved in the NO_2 adsorption for the formation of nitrates.

Nitrate route:

$$BaO + 3\ NO_2 \leftrightarrow 2\ Ba(NO_3)_2 + NO \quad (3)$$

NO_x disproportionation

$$BaO + 2NO_2 \leftrightarrow Ba(NO_2)(NO_3) \quad (3.1)$$

$$Ba(NO_2)(NO_3) + NO_2 \leftrightarrow Ba(NO_3)_2 + NO \quad (3.2)$$

reaction involving the formation of barium peroxide

$$BaO + NO_2 \leftrightarrow BaO(O) + NO \quad (3.3(R31))$$

$$BaO(O) + 2NO_2 \leftrightarrow Ba(NO_3)_2 \quad (3.4)$$

While the global reactions of nitrite route[25] which is in parallel to nitrate route are presented in Equations 4 and 5[9]. NO can be directly adsorbed as nitrite on Ba sites with help of Pt showed in Equation 4, then Ba(NO2)2 are further oxidized to stable nitrates by the spilled over oxygen from Pt sites showed in Equation 5. The global reaction 4 and 5 can be derived by elementary reaction R11, R12, R13, R33, R34, R35 and the reverse reaction of R41. In this study, $Ba(NO_3)_2$ site fraction and $BaO\text{-}NO_2$ site fraction are employed to characterize two kinds of NO_x adsorption pathways. It is noting that $Ba(NO_3)_2$ can be obtained from both nitrate route as indicated in Equation 3.1~3.4 and intermediate production conversion (nitrite route) showed in Equations 4~5. Therefor nitrate route can be indicated as difference between total $Ba(NO_3)_2$ site fraction and the part of $Ba(NO_3)_2$ produced by nitrite route, i.e., the $BaO\text{-}NO_2$ site fraction in consideration of relationship of stoichiometric number showed in Equation 5.

Nitrite route:

$$BaO + 2NO + 0.5O_2 \leftrightarrow Ba(NO_2)_2 \quad (4)$$

$$Ba(NO_2)_2 + O_2 \leftrightarrow Ba(NO_3)_2 \quad (5)$$

The Figure 2 illustrates the overall perspective of reaction path related to NO_x storage to get more intuitive understanding. There were not arrows in connecting lines between species because the reactions between these species are reversible as shown in Table 3. Table 3 also gives the forward and reverse kinetic parameters for each reaction, i.e., the values of A_i, β_i, and E_i in the generalized Arrhenius expression

$$k_i = A_i T^{\beta_i} e^{\frac{-E_i}{RT}} \quad (6)$$

where A_i is the pre-exponential factor, β_i is the temperature exponent, and the activation energy is E_i.

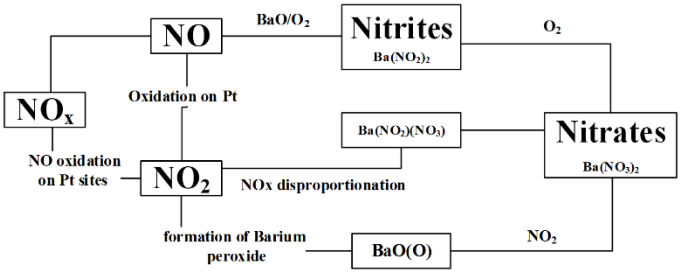

Fig. 2. Diagrammatic NO_x storage routes.

3.3 Modelling Validation

There are 44 reactions in total involved in LNT-EGR kinetics model, which is comprised of several sub-model mentioned in section 3.2 including NO oxidation, oxidation of reductants CO, NH_3 and H_2, NO_x storage including both nitrate and nitrite routes, water–gas shift reaction, water decomposition reaction, formation of NH_3 and N_2O, intermediate products surface isocyanate reaction, spillover process of NO_2 and reduction reaction of stored NO_x. These sub-models which are from different research groups' work as mentioned above were picked up here to combine final LNT-EGR model. Parameter values (pre-exponential factor, temperature exponent and the activation energy) of NO oxidation rate expressed by R1, R2, R6 and R13 are from the NO_x adsorption experiments lasting long enough to show almost full NO_x breakthrough conducted by Kočí P, Marek M et al.[26] Parameter values of oxidation of reductants CO, H_2 and NH_3 expressed by R8, R15, R19 were from the CO, H_2 and HC oxidation light-off experiments based on slow temperature ramps under both lean and rich conditions at different con-centration levels conducted by Kočí P, Schejbal M et al.[27] These literature parameters values of these sub-models were used as the initial guess and followed by tuning to get a reasonable fitting for each sub-model. The Figure 3 illustrates the overall perspective of reaction path related to sub-models to get more intuitive understanding.

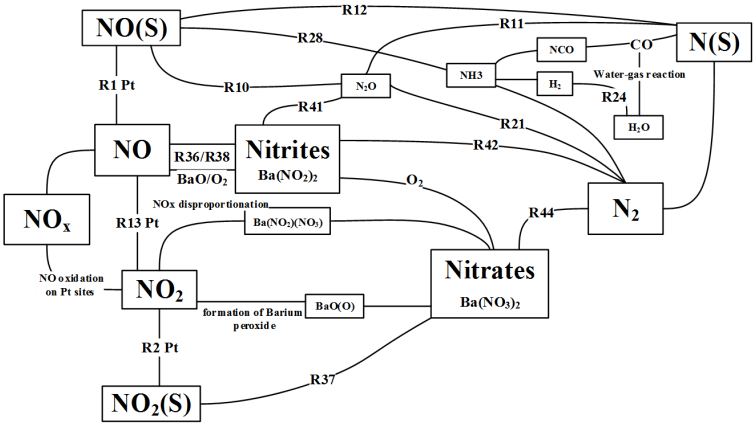

Fig. 3. Diagrammatic NO_x storage and reduction reaction path。

After the preliminary determination of sub-model, the whole performance of LNT under different EGR rate was validated by the lean-burn gasoline engine test bench as we mention

above. Considering the simulation accuracy and calculation cost, the step size for setting the simulation calculation is 0.1 s. In order to verify the accuracy of the model, the exhaust conditions of the catalyst under the different EGR rates measured in the previous experiment are used as the simulated boundary conditions of the catalyst. According to the engine exhaust components and concentrations measured by the experiment, the catalyst inlet gas concentration and other boundary conditions were obtained. For the comparative study, the EGR rates are set as 0%, 10%, 15%, 20%, 25%, 30%, respectively. Corresponding gas compositions and concentrations are shown in Table 2 as mentioned in Experiment setup. The comparison of outlet NO_x slip between simulation and experiment is shown in Figure 4. It can be found that NO_x slip of LNT from chemical reaction kinetics simulation has the similar trend with the experimental results. Simulation values basically can represent outlet NO_x slip because of catalyst desorption, adsorption saturation and storage site limitation. As shown in Figure 4, the error between simulation and experiment is about 50ppm when the EGR is below 10%, when EGR increases up to 15% the error decreases below 30ppm, which indicated that maximum relative error between simulation and experiment is 4.5%, which is lower than 5%. The error may come from the distance between measurement point of LNT outlet and HORIBA gaseous element analyzer, LNT still has adsorption ability as engine switches into rich-burn phase, and abundant desorption has delay. Meanwhile, experimental catalyst cannot switch from lean-mode to rich-mode instantaneously, but simulation can switch immediately, so the simulation has more NO_x slip because of desorption. All in all, these verify the validity of the mechanism so the LNT-EGR model can be used for further investigate.

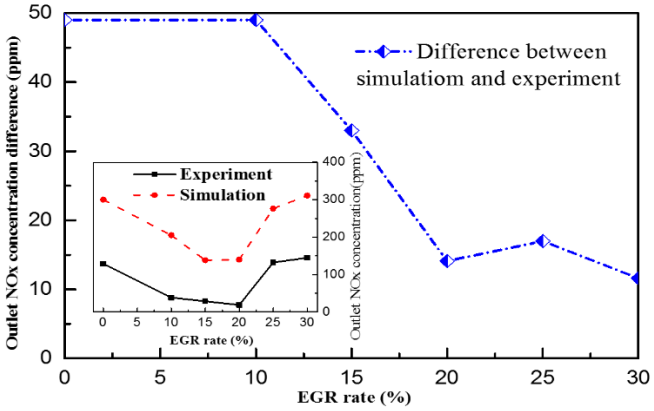

Fig. 4. Comparison of simulation and experiment of LNT.

4 Results and discussion

4.1 Effects of EGR rate on NO_x storage at fixed temperature

Effects of EGR rate on NO_x storage process were studied by the contributions and variation tendencies of the two different NO_x adsorption pathways, i.e., nitrate route and nitrite route. The nitrate route and nitrite route are characterized by $Ba(NO_3)_2$ and $BaO\text{-}NO_2$ site fractions, respectively. As previously mentioned, noting that nitrates are accumulated by both nitrate route as indicated in Equation 3.1~3.4 and intermediate production conversion (nitrite route) showed in Equations 4~5. The temperature was set as 350℃.

The main reason of the EGR effects on LNT overall performance is the change of concentration and ratio of inlet components CO_2\H_2O as mentioned in Introduction. Before the discussion of EGR effects on NO_x storage pathway, it should be aware of that the

combined influences of both CO_2 and H_2O on NO_x storage and reduction are not equivalent to the individual effects of CO_2 or H_2O. In this paper, combined influences of both CO_2 and H_2O on NO_x storage are discussed in the level of EGR, as a matter of convenience for analysis, the trend of CO_2 and H_2O concentration from raw emission under different EGR rate at 350℃ was showed in Figure 5.

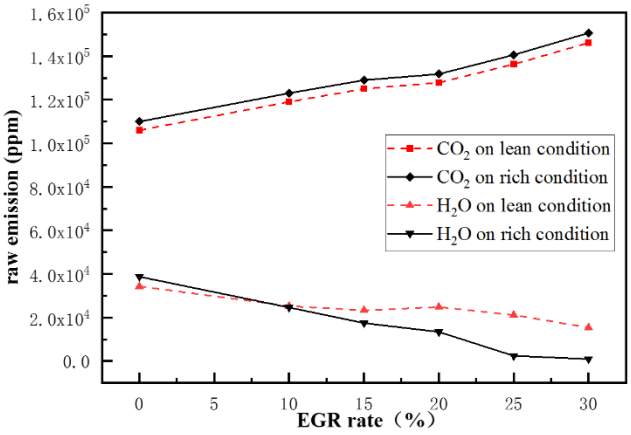

Fig. 5. Trend of CO_2 and H_2O concentration from raw emission under the different EGR rate at 350℃.

Figure 6 shows time-varying $Ba(NO_3)_2$ site fraction under different EGR rates at 350℃. EGR rates are divided into two intervals of 0%~15% and 20%~30% due to the different variation tendency of $Ba(NO_3)_2$ site fraction. When the EGR rate increases from 0% to 15%, $Ba(NO_3)_2$ site fraction decreased gradually, which indicates that increase of EGR rate shows inhibition effects on the NO_x storage as $Ba(NO_3)_2$. Taking the 350 s of the adsorption stage as an example, when the EGR rate increases from 0% to 10%, $Ba(NO_3)_2$ site fraction is reduced by 6.78%, while EGR rate increased from 10% to 15%, $Ba(NO_3)_2$ site fraction is reduced by 8.58%. Therefore, inhibition of EGR on stored $Ba(NO_3)_2$ slightly aggravates with the EGR rate increase. This is because CO_2 concentration of inlet increased with EGR rate as showed in Figure 5, resulting in production of $BaCO_3$ from the reaction R29 ($CO_2 + BaO \leftrightarrow BaCO_3$) which indicated CO_2 was chemisorbed on the BaO sites leaded to reduction of entire NO_x storage sites. The result was in line with Epling W S et al.[13] study mentioned before. In addition, it's more difficult for NO_x absorbed on $BaCO_3$ than BaO[14] due to high thermal stability of $BaCO_3$, which leads to reduction of $Ba(NO_3)_2$ production as well. The effects of H_2O on NO_x storage process is neglected not only because its concentration of inlet decreases with EGR rate, but also H_2O playes a much weaker role in NO_x adsorption, which is widely reported in literatures such as reference[13]. The role of H_2O is practiced not so much in NO_x adsorption as in formation of NH_3 and N_2O through water-gas shift reaction and subsidiarity of reactions involving intermediate products such as -NCO, -H and -OH, which would be discussed later.

When the EGR rate increases within interval of 20%~30%, $Ba(NO_3)_2$ site fraction continues decreasing, maintaining range of 15%~25%, and the change amplitude significantly reduced. At moment of 150 s, when the EGR rate increased from 20% to 25% and from 25% to 30%, $Ba(NO_3)_2$ site fraction reductions are 0.18% and 0.34%, respectively. EGR still shows inhibition effect but the degree weakens. The distinctly different $Ba(NO_3)_2$ site fraction trends of the two EGR intervals of 0%~15% and 20%~30% are on account of the equilibrium limitations of reaction R29, which reveals competing adsorption mechanism of CO_2, i.e., the same NO_x storage sites (Ba sites) are occupied by CO_2. Therefore, reduction

of $Ba(NO_3)_2$ site fraction with increased EGR rate of intervals 20%~30% became less pronounced, through concentration of CO_2 continuously increased with EGR rate.

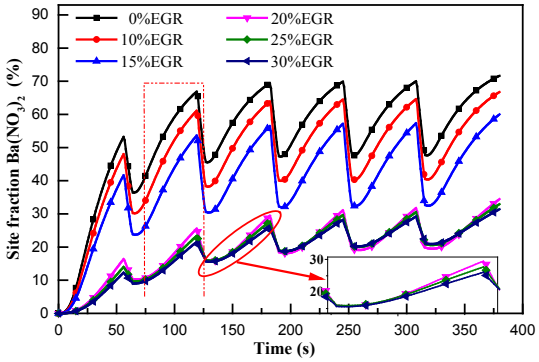

Fig. 6. Time-varying $Ba(NO_3)_2$ site fraction under different EGR rates at 350℃.

Figure 7 shows the time-varying trend of $BaO\text{-}NO_2$ site fraction which is different from the $Ba(NO_3)_2$ site fraction under varying EGR rate within range of 0%~30% with 5% increment. Noting the line groups inside the red dashed boxes of the figure 7 and figure 6, time interval 64s~119s is selected for comparison. $Ba(NO_3)_2$ site fraction shows a tendency of rise while the BaO-NO2 site fraction trend is drop in the same time interval. Contacting the figure 6, the time-varying trends of site fraction for both nitrates and nitrites are complementary because of the fixed NO_x storage sites due to the limitation of commercial LNT catalytic converter.

When the EGR rate increases from 0% to 15%, the nitrite site fraction is reduced first and increases later in the NO_x storage stage such as time interval 0s~56s, however the later increase of $BaO\text{-}NO_2$ site fraction became more evident and stable in subsequent cycles while the first reduction of $BaO\text{-}NO_2$ site fraction with EGR rate increasing was negligible. Hence EGR shows early slightly inhibition and later promotion on the nitrite path in the EGR interval of 0%~15%. At the 350s of the adsorption stage, the $BaO\text{-}NO_2$ site fraction respectively increases by 4.56% and 5.6% as the EGR rate increased between the two EGR rate intervals 0%~10% and 10% ~15%, which shows positive effects of EGR on the nitrite path slightly aggravating with the increase of the EGR rate as the cycle was stabilized. There is different situation as EGR rate varies in the interval 20%~30%, the $BaO\text{-}NO_2$ fraction marginally decreases with the increasing EGR rate in the NO_x storage stage, and increases in flowing NO_x reduction stage. The $BaO\text{-}NO_2$ site fraction is reduced only by 1.08% and 0.81%, respectively for two EGR rate intervals 20%~25% and 25% ~30%, which shows the weak correlation between the $BaO\text{-}NO_2$ site fraction and EGR rate interval 20%~30%. The high overlap of the lines group of EGR rate interval 20%~30% in Figure 7 also underlines this point. The main reason of the difference between two EGR rate intervals (0%~15% and 20%~30%) above is that the reduction of Ba sites occupied by CO_2 was stabilized due to equilibrium limitations of reaction R29.

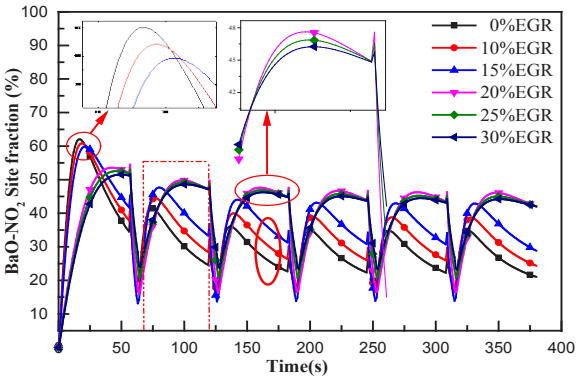

Fig. 7. BaO-NO_2 site fraction under different EGR rates at 350℃.

In addition, it can be clearly seen that two trends of $Ba(NO_3)_2$ and BaO-NO_2 site fraction are less stable in the first cycle of the simulation from Figure 6 and 7. Furthermore, both $Ba(NO_3)_2$ and BaO-NO_2 site fraction of first cycle are different from the corresponding flowing cycle, $Ba(NO_3)_2$ site fraction is lower while BaO-NO2 site fraction is higher. This phenomenon indicates that nitrite route represents the major storage during the initial NO_x storage in the presence of NO_x and O_2 mixtures under lean condition.

As for variation of $Ba(NO_3)_2$ site fraction, nitrates are the final products of stable storage of NO_x as showed in the Figure 2 (diagrammatic NO_x storage routes) at 350 °C. $Ba(NO_3)_2$ site fraction of each adsorption cycle consists of residual part from last cycle and production part of current ongoing cycle except for the first cycle which has the largest quantity of fresh NO_x adsorption sites. Nitrite route and nitrate route concurrently accomplish the NO_x storage, but BaO-NO_2 is intermediate product of the unstable nitrite route, which is in the process of continuous production and transformation. It takes long storage times to oxidize nitrites to nitrates with help of oxygen and Pt sites. Therefore, in the first adsorption cycle there is lower $Ba(NO_3)_2$ site fraction than following cycles because of the absence of residual nitrates from last cycle and less production of nitrates came from oxidized nitrites for being pressed for time. Initial instability of site fraction is attributed to the largest quantity of fresh NO_x adsorption sites of first cycle mentioned above. As for the situation of BaO-NO_2 site fraction can be explained by the complementary correlation between nitrate route and nitrite route mentioned before.

Figure 8 shows the trend of $Ba(NO_3)_2$ and BaO-NO_2 site fraction at 0% EGR rate. During the adsorption phase of each cycle, the $Ba(NO_3)_2$ site fraction shows a continuous increasing trend, i.e., NO_x is continuously stored as stable nitrates through several different reaction pathways including NO_x disproportionation, reaction involving the formation of barium peroxide and nitrite route expressed by Equation 4~5. It's worth noting that BaO-NO_2 site fraction only increases at the beginning of each NO_x adsorption phase, and the increase rate is significantly higher than the $Ba(NO_3)_2$ site fraction. During the late phase of adsorption, BaO-NO_2 fraction decreases over adsorption time until the adsorption phase completed, which has confirmed the conversion process of nitrite route due to BaO-NO_2 further oxidized to nitrates leading to corresponding increase of $Ba(NO_3)_2$ site fraction. Therefore, the time-varying NO_x storage process under lean condition at fixed temperature (350℃) can be concluded as follows, both nitrate and nitrite storage routes proceed simultaneously and parallelly, more Ba sites are occupied though nitrite process (Equation 4 and Equation 5) at the initial NO_x uptake. As time marching on, stored BaO-NO_2 is oxidized to $Ba(NO_3)_2$ in the lean atmosphere of storage stage. Combining NO_x disproportionation (Equation 3.1 & Equation 3.2) reaction involving the formation of barium peroxide (Equation 3.3 & Equation 3.4), $Ba(NO_3)_2$ site fraction rises rapidly while BaO-NO_2 site fraction drops accordingly due

to the conserved Ba sites. Taking the adsorption phase of the third stable cycle as an example, the $Ba(NO_3)_2$ site fraction increases by about 23.73%, of which about 13.37% is derived from the nitrite route. Hence the occupancy ratio of NO_x storage sites through the nitrate path and the nitrite path acquired by calculation is about 1:1.63, which indicated the corresponding contribution of nitrate route and the nitrite route to NO_x storage at 0% EGR rate.

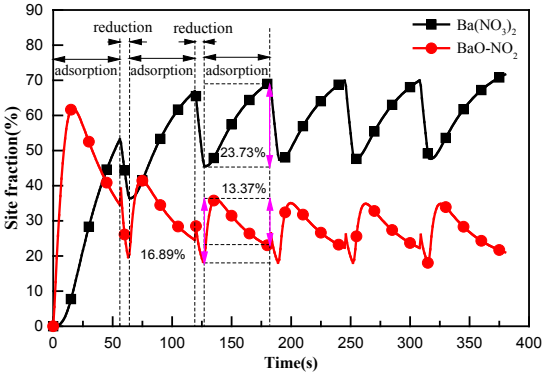

Fig. 8. $Ba(NO_3)_2$ site fraction and $BaO\text{-}NO_2$ site fraction under 0% EGR rate at 350℃.

The similar NO_x storage processes under other EGR rates would not be repeated here for saving space. However, the difference of NO_x storage performance with EGR changing and the contributions to NO_x storage of both nitrate and nitrite route, which are expressed as ratio of NO_x storage sites occupied through the two different adsorption routes, were discussed below.

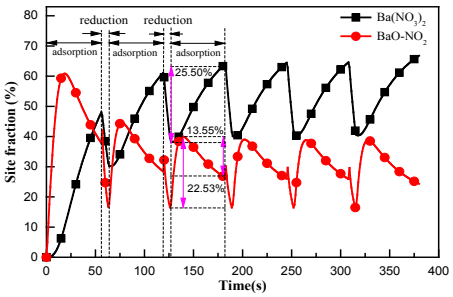

Fig. 9. $Ba(NO_3)_2$ site fraction and $BaO\text{-}NO_2$ site fraction under 10% EGR rate at 350℃.

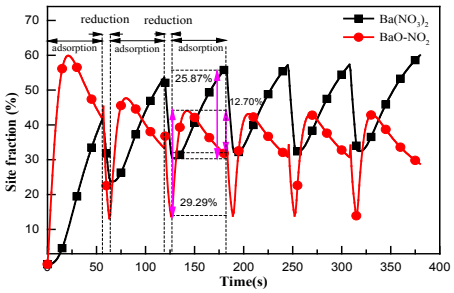

Fig.10. $Ba(NO_3)_2$ site fraction and $BaO\text{-}NO_2$ site fraction under 15% EGR rate at 350℃.

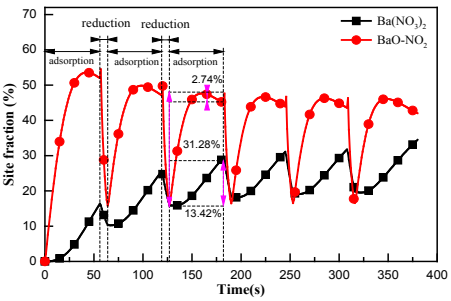

Fig. 11. $Ba(NO_3)_2$ site fraction and $BaO\text{-}NO_2$ site fraction under 20% EGR rate at 350℃.

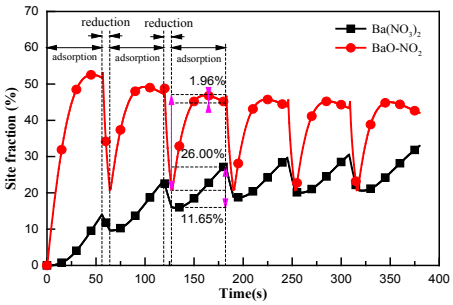

Fig. 12. $Ba(NO_3)_2$ site fraction and $BaO\text{-}NO_2$ site fraction under 25% EGR rate at 350℃.

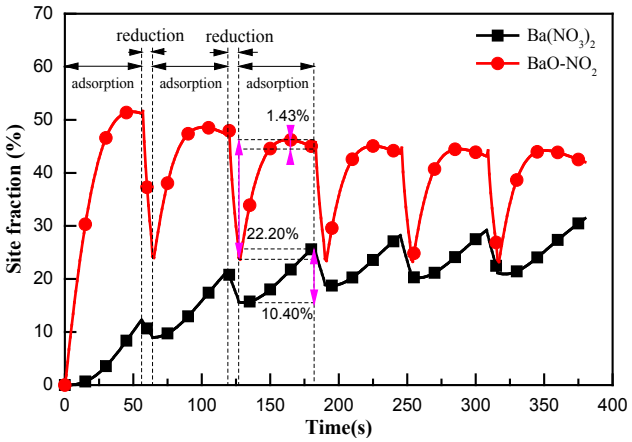

Fig. 13. $Ba(NO_3)_2$ site fraction and $BaO\text{-}NO_2$ site fraction under 30% EGR rate at 350℃.

For analysis of other EGR rates set, the third lean-burn cycle is selected for the rest EGR rate as 0% EGR rate did in consideration of controlling variable to minimize errors as much as possible. Figure 9 shows the time variable $Ba(NO_3)_2$ site fraction and $BaO\text{-}NO_2$ site fraction of 10% EGR rate, the Ba(NO3)2 increases by 25.50% and the corresponding $BaO\text{-}NO_2$ reduction was 13.55% during the third cycle. Therefore, the percentage of NO_x storage sites occupied through nitrate route and the nitrite route accounts for 11.95% and 22.53%, respectively, with a view to the Ba sites consumed by CO_2 (R29) and the Ba sites at inactivated state. Hence the ratio of nitrate route to the nitrite route is about 1:1.89. In the third lean-burn cycle corresponding to 15% EGR showed in Figure 10, the $Ba(NO_3)_2$ site fraction increase is 25.87%, and the corresponding BaO-NO2 fractional decrease is 12.70%. Nitrate path and nitrite path accounted for 13.17% and 29.29%, respectively. The ratio of the two routes is about 1:2.22. Similarly, the percentage of NO_x storage sites occupied through nitrate route and the nitrite route under EGR rate of 20%, 25% and 30% could be calculated by the data showed in Figure 11, 12 and 13, respectively. Therefore, the respective ratios of nitrate route to the nitrite route of each EGR rate above are 1:2.92, 1:2.68 and 1:2.47.

The ratio of nitrate route to nitrite route and Ba sites occupation of two NO_x storage pathways with EGR rate changing are showed in Figure 14. It's worth noting that the connection and difference between the site fraction of $Ba(NO_3)_2$ and the nitrate route. For a better understanding of the leading role of both NO_x adsorption routes with EGR changing, nitrate route is separated by subtracting the $Ba(NO_3)_2$ produced by nitrite route, which is equivalent to the amount of $BaO\text{-}NO_2$ involved in the nitrite oxidation reaction in consideration of relationship of stoichiometric number showed in Equation 5, from total Ba(NO3)2 production.

In the range of 0% ~ 20% EGR rate, the ratio of nitrate route to nitrite route drops while raises in the 20% ~ 30% EGR rate. With EGR rate changing from 0%~30%, there is slight variation of occupation of Ba sites by nitrate route whereas Ba sites occupation by nitrite route isn't at the operating temperature (350℃). Furthermore, similar trend of Ba sites occupation of both two NO_x storage pathways is showed in Figure 14, which raises first and drops later. The change of ratio of nitrate route to nitrite route is decided by nitrite route to a great extent due to slight variation of occupation of Ba sites by nitrate route as showed above. Only when CO_2 concentration reaches to a certa in quantity such as the amount contented in high EGR rate over 15%, its inhibition on NO_x storage process begins to emerge, though the reaction R29($CO_2 + BaO \leftrightarrow BaCO_3$) of CO_2 competitive adsorption on the Ba sites and NO_x storage reaction coexisted. Both nitrate and nitrite routes are unaffected by increased CO_2

quantity within the range of low EGR rate due to abundant Ba sites for both NO_x and CO_2 adsorption. In the meantime, the amount of CO from engine exhaust raised modestly with EGR rate increase, which facilitates chemical equilibrium of reversible reaction R40 ($Ba(NO_3)_2 + CO(S) \leftrightarrow BaO(NO_2) + NO_2 + CO_2 + Pt(S)$) shifting to the right leading to more $BaO\text{-}NO_2$ production. Meanwhile, the reduction of water steam with EGR rate increase shifts the chemical equilibrium of reversible reaction R36($BaO(NO_2) + H(S) \leftrightarrow BaO + NO + OH(S)$) to left resulting more $BaO\text{-}NO_2$ formation. Water steam reduction is not conducive to chemical equilibrium of reversible reaction R37($Ba(NO_3)_2 + H(S) \leftrightarrow BaO(NO_2) + NO_2 + OH(S)$) due to both H(S) and OH(S) came from hydrolysis reaction which is reverse reaction of R14($H(S) + OH(S) \leftrightarrow H_2O(S) + Pt(S)$) with presence of catalyst Pt sites. Therefore, Ba sites occupation by nitrite route raises in range of 0%~20% EGR rate as well as nitrate route because of more NO_2 formation through reaction R23($NO_2(S) + CO(S) \leftrightarrow NO(S) + CO_2 + Pt(S)$) with the help of increased CO_2 quantity with EGR rate increased.

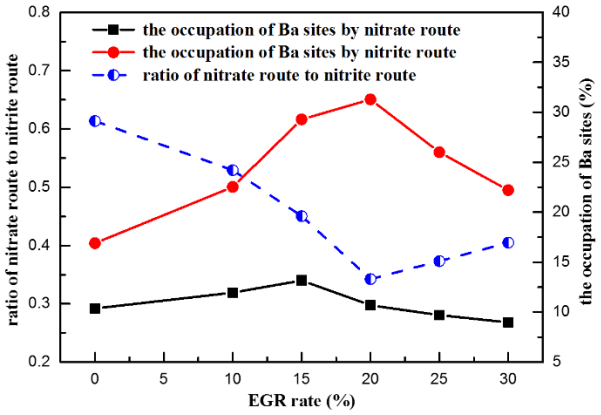

Fig. 14. ratio of nitrate route to nitrite route and Ba sites occupied by the two NO_x storage pathways under different EGR rate at 350℃.

4.2 Effects of EGR rate under different temperature zone

Temperature is vital for chemical reaction as is well-known. The case of variation for nitrate route and nitrite routs under different EGR rate is discussed at a fixed typical LNT operating temperature 350℃ above. Performance of EGR (0%,10%,15%,20%,25%) effects on NO_x storage course at varying temperatures would be talked about below. According to actual engine operation conditions with different EGR rates, the simulations were carried out at different inlet temperatures from 150℃ to 550℃. For the sake of clearer interpretations, the numerical results were divided into three temperature zones: low temperature zone, i.e., 150℃ ~200℃, moderate temperature zone, i.e. 250℃~400℃, and high temperature zone, i.e. 450℃ ~550℃.

4.2.1 In low temperature zone

The time-varying variation trend of $Ba(NO_3)_2$ and $BaO\text{-}NO_2$ site fraction under different EGR rate at low temperature zone (150℃~200℃) is showed in Figure 15.

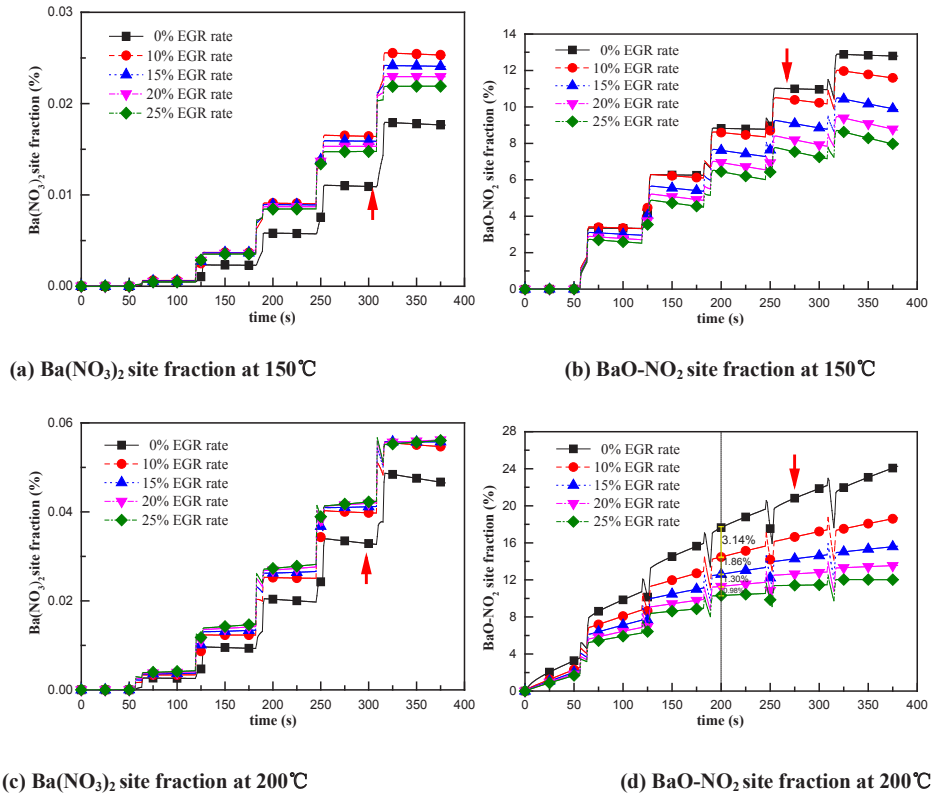

(a) $Ba(NO_3)_2$ site fraction at 150℃ **(b) $BaO\text{-}NO_2$ site fraction at 150℃**

(c) $Ba(NO_3)_2$ site fraction at 200℃ **(d) $BaO\text{-}NO_2$ site fraction at 200℃**

Fig. 15. $Ba(NO_3)_2$ and $BaO\text{-}NO_2$ site fraction under different EGR rate at Low temperature.

As showed in Figure 15, the $Ba(NO_3)_2$ site fraction is no more than 0.06% in terms of simulation results while the maximum $BaO\text{-}NO_2$ site fraction is about 25% over the whole low temperature range, which indicates that $Ba(NO_3)_2$ site fraction is far less than $BaO\text{-}NO_2$ site fraction. Therefore, the nitrite route dominates the NO_x storage at low temperature zone in a very explicit way. The primary cause is little NO_2 which is essential for nitrates formation produced from NO oxidation because NO oxidation reaction R13($NO(S) + O(S) \leftrightarrow NO_2(S) + Pt(S)$) is kinetically limited at low temperature, especially near 150℃ (with about maximum 0.025% Ba(NO3)2 site fraction), which is in line with experimental results from Olsson L[28]. Note that the change of left scale of figure 15 (a) and (c) indicates that $Ba(NO_3)_2$ site fraction doubled due to increasing temperature from 150℃ to 200℃. Meanwhile $BaO\text{-}NO_2$ site fraction increased with temperature increasing as well through comparison of $BaO\text{-}NO_2$ site fraction under same EGR rate but different temperatures as showed in Figure 15 (b) and (d).

Because of negligible amounts of the $Ba(NO_3)_2$ site fraction, the effects of EGR rate and temperature on the $BaO\text{-}NO_2$ site fraction (nitrite route) are mainly discussed below. As showed in Figure 15 (b) and (d), the $BaO\text{-}NO_2$ site fraction decreases with the increase of EGR rate at both 150℃ and 200℃ for the CO_2 competitive adsorption reason as mentioned before. The increase of $BaO\text{-}NO_2$ site fraction slows down as the EGR rate increase, which is more obvious at inlet temperature of 200℃ as showed in Figure 15 (d). This is because the consumption rate of Ba sites taken for initially appeared nitrites and negligible nitrates is stable over storage time because impacts of kinetically limitation of NO oxidation fade away with temperature increase within 150℃~200℃, leading to reduction of NO and

corresponding nitrites. As showed in Figure 15 (d) when the EGR rate increases from 0% to 10% at 200℃, the BaO-NO_2 site fraction drops approximately 3.14% at 200 s. For EGR rate increases from 10% to 25% with increment 5%, the calculations of the variation degree are conducted at 200 s as well, and the corresponding decline of BaO-NO_2 site fraction is about 1.86%, 1.30%, 0.98%, respectively for different EGR rate intervals. So, the inhibition degree of EGR rate on nitrite route weakens with EGR rate increased at 200℃, because CO_2 adsorption competitiveness gradually reaches to saturation with incremental EGR rate.

4.2.2 In moderate temperature zone

Figure 16 shows the variation trend of $Ba(NO_3)_2$ and BaO-NO_2 site fraction over time under different EGR rate at moderate temperature zone (250℃~400℃).

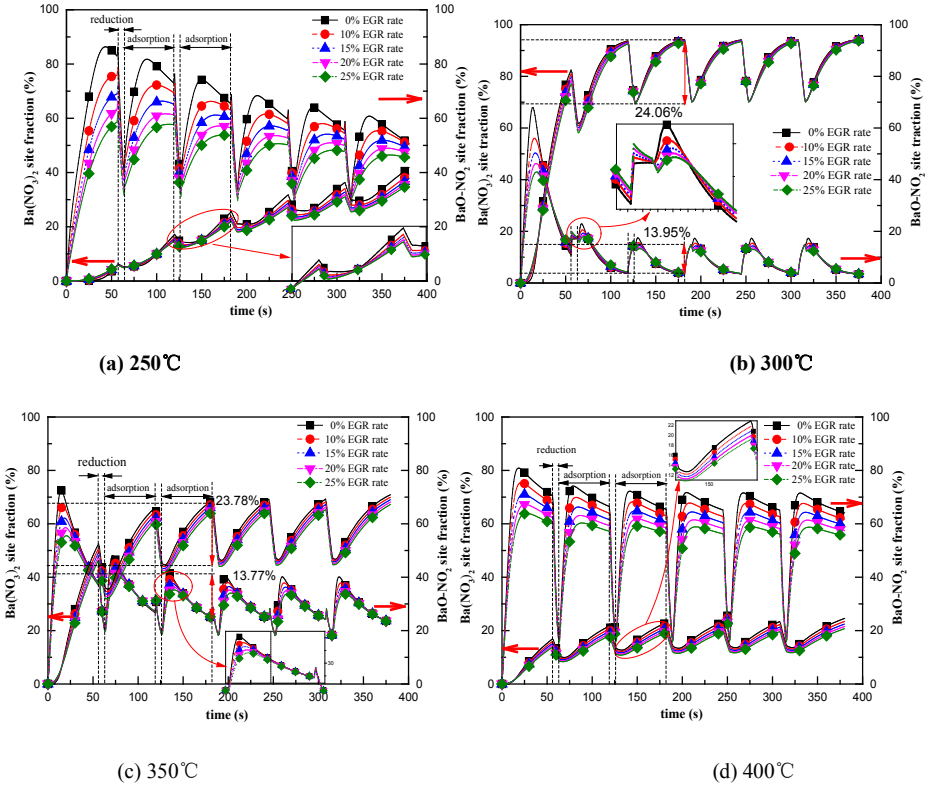

Fig. 16. $Ba(NO_3)_2$ site fraction and BaO-NO_2 site fraction under different EGR rate at moderate temperature.

With the increase of temperature from low temperature zone to moderate temperature zone, both of the $Ba(NO_3)_2$ and BaO-NO_2 site fraction increases significantly, especially the $Ba(NO_3)_2$ site fraction. Take 10% EGR rate as an example, the maximum $Ba(NO_3)_2$ site fraction is about 40% as showed in Figure 11 (a) at 250℃. For the temperature of 300℃, 350℃ and 400℃, the maximum $Ba(NO_3)_2$ site fraction is about 95%, 70% and 25%, respectively. Visibly from Figure 16 (a)-(d) with temperature raises from 250℃ to 400℃, the $Ba(NO_3)_2$ site fraction increases first and declines later and BaO-NO_2 site fraction trend changed oppositely at moderate temperature zone which is major turning point for NO_x storage pathway conversion and change. Furthermore, $Ba(NO_3)_2$ site fraction increases by

24.06% under 10% EGR rate as showed in Figure 16 (b), in the adsorption phase (127~182 s). Meanwhile, BaO-NO_2 site fraction decreases by 13.95%. $Ba(NO_3)_2$ can be obtained from both nitrate and nitrite routes as showed in Figure 2 (diagrammatic NO_x storage routes). Therefore, at 300℃ the probabilities of nitrate path and nitrite path were 10.11% and 13.95%, respectively. And at 350℃, the probabilities of nitrate path and nitrite path were about 10.01% and 13.77%. So, the two adsorption pathways have approximately equivalent contribution to NO_x storage at 300℃and 350℃.

The cause of nitrate route participation raises first to reach same level of BaO-NO_2 site fraction and drops later is result of comprehensive effects of NO oxidation thermodynamic restriction, nitrate and nitrite thermostability and conversion between nitrites and nitrates. With temperature increasing from 250℃ to 350℃, there is an interval between kinetically limitation vanished and thermodynamic restriction appeared during which NO_2 production from NO oxidation (R13 NO(S) + O(S) ↔ NO_2(S) + Pt(S)) is at the highest level, which is in accordance with study of Olsson L[28]. NO_x disproportionation (BaO + $3NO_2$ ↔ $Ba(NO_2)(NO_3)$(3.1) & $Ba(NO_2)(NO_3)$ + NO_2 ↔ $Ba(NO_3)_2$ + NO(3.2)) is more and more important with temperature raised within the interval (250℃~ 350℃) leading to more nitrates formation. Hence nitrate route participation raises first from 250℃ to 350℃ based on above two primary reasons. The absolute amount of nitrates which can be seen through $Ba(NO_3)_2$ site fraction value in figure 16 (b) and (c) was at very high level at 300℃ and 350℃ due to formation of barium nitrate species from nitrite species ($Ba(NO_2)_2$ + O_2↔ $Ba(NO_3)_2$ (Equation5)) with Pt catalyzing is optimum in this temperature range (300℃~350℃) which is also reported by Forzatti P[29].

As the temperature subsequently raises to 400℃, reduction of nitrates generation from NO_2(BaO + 3 NO_2 ↔ 2 $Ba(NO_3)_2$ + NO (Equation3)) due to thermodynamics limitation of NO oxidation above 350℃ and decline of stored nitrates due to thermal instability of nitrates at high temperature like 400℃ result in decrease of $Ba(NO_3)_2$ site fraction above 350℃ of moderate temperature zone. Meanwhile the variation tendency of BaO-NO_2 site fraction is opposite to $Ba(NO_3)_2$ site fraction variation for the reason of NO_x storage sites (Ba sites) conservation and complementary correlation between nitrate and nitrite route mentioned before.

In additional, there are fluctuations of BaO-NO_2 site fraction during the switching between rich and lean condition as showed in partial enlarged detail highlighted in red circle of figure 16 (b). These fluctuations came from the change of equilibrium and rates of reactions (BaO + 3 NO_2 ↔ 2$Ba(NO_3)_2$ + NO (Equation3), BaO + 2NO + 0.5O_2↔ $Ba(NO_2)_2$ (Equation4) and $Ba(NO_2)_2$ + O_2↔ $Ba(NO_3)_2$ (Equation5)) which are affected greatly by local concentration of NO, NO_2 and O_2. The rich-lean switch leads to changes in NO, NO_2 and O_2 local concentrations and the ratio of arbitrary two of these species.

4.2.3 In high temperature zone

The variation tendency of $Ba(NO_3)_2$ and BaO-NO_2 site fraction over time under different EGR rate at high temperature zone (450℃~550℃) is showed in Figure 17. taking notice of different scale of left and right Y axis in Figure 17 (a), (b) and (c). It can be clearly seen that $Ba(NO_3)_2$ site fraction is no more than 5% whereas BaO-NO_2 site fraction maintained at a very high level, which indicates that nitrite route dominates again with temperature raises to high temperature zone as a result of the reduction of nitrates formation and nitrates pyrolysis at high temperature. As mentioned before, NO oxidation is thermodynamic limited above 350℃[28] resulting in reduction of formation of NO_2 which is crucial reactant for nitrates formation through BaO + 3 NO_2 ↔ 2 $Ba(NO_3)_2$ + NO (Equation3), leading to reduction of

nitrates formation. Meanwhile the degradation of thermal stability of nitrates resultes in reduction of stored nitrates through reaction R33 (NO_2 + $BaO(NO_3)$ ↔ $Ba(NO_3)_2$). In addition, $Ba(NO_3)_2$ from nitrite route also decreases because last reaction step of nitrite route ($Ba(NO_2)_2 + O_2$↔ $Ba(NO_3)_2$(Equation5)) is affected by thermodynamic limitation above 350℃ [29]. As EGR rate increases from 0% to 25%, both of $Ba(NO_3)_2$ and BaO-NO_2 site fraction decreases in high temperature zone which is similar with tendency of low and moderate temperature zone except for the special circumstance of $Ba(NO_3)_2$ site fraction under 0% EGR rate at 150℃ and 200℃ explained before. The decline degree of $Ba(NO_3)_2$ and BaO-NO_2 site fraction decreases with EGR rate increasing, because CO_2 adsorption competitiveness gradually reaches to saturation with increasing EGR rate.

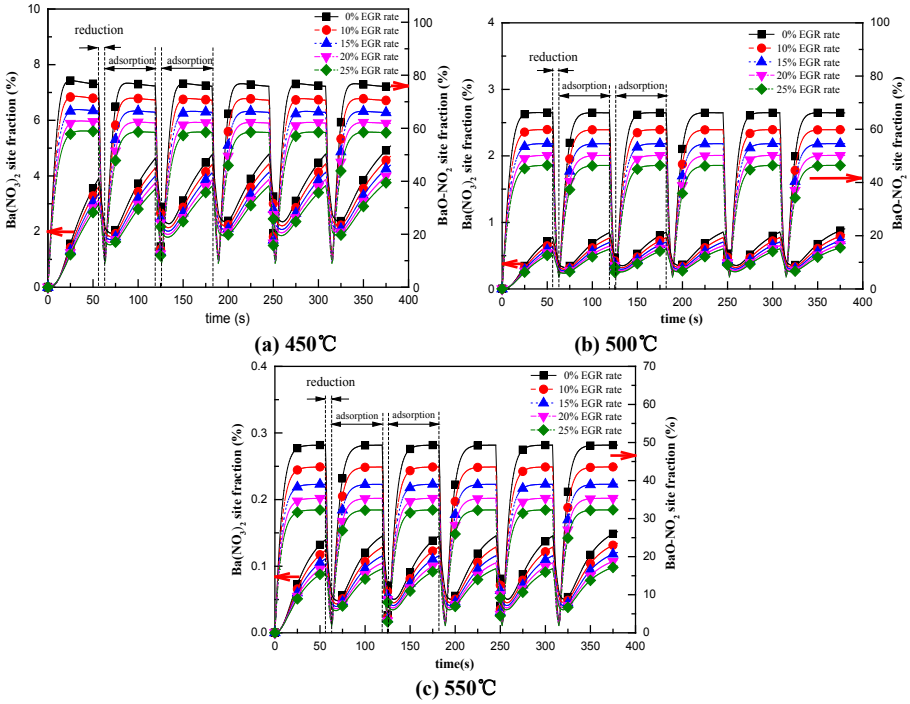

Fig. 17. $Ba(NO_3)_2$ site fraction and BaO-NO_2 site fraction under different EGR rate at high temperature.

5 Conclusion

A LNT model coupled with EGR was developed based on the Langmuir–Hinshelwood mechanism to investigate the EGR effects on NO_x adsorption pathway of LNT catalysts with temperature changed in range 150℃~550℃. Both the nitrate and nitrite adsorption paths were considered for the NO_x storage process in the model as well as the spillover of stored NO_x between Ba and Pt sites. The model quantified the contributions of both nitrate route and nitrite route to the NO_x storage capacity for LNT with change of EGR rate (0%~30%) at fixed temperature under raw emission atmosphere from tested gasoline engine.

At fixed inlet temperature of 350℃ set for high NO_x conversion efficiency, EGR rate shows restraining effects on $Ba(NO_3)_2$ site fraction within range of 0%~30% whereas promotion effects on BaO-NO_2 site fraction from 0% to 15% and inhibition effects in subsequent EGR rate 20%~30%. There is opposite tendency between $Ba(NO_3)_2$ site fraction BaO-NO_2 site fraction over time in the same cycle of operation due to the complementary

correlation between nitrate route and nitrite route. Furthermore, the similar trends of site fraction assorted in EGR rate interval 0%~15% were different from the similar trends of site fraction which were assorted in EGR rate interval 20%~30% for both $Ba(NO_3)_2$ site fraction and BaO-NO_2 site fraction due to the equilibrium limitations of the reaction about CO_2 was chemisorbed on the BaO sites which are supposed to be occupied by NO_x. As for contributions of the two routes to NO_x storage, in the range of 0% ~ 20% EGR rate, the ratio of nitrate route to nitrite route dropped while raised in the 20% ~ 30% EGR rate, the ratio is decided by nitrite route to a great extent due to slight variation of occupation of Ba sites by nitrate route due to great cardinal number of NO amounts from raw engine emission, thermodynamics limitation of NO_x oxidation and in part thermal decomposition of stored $Ba(NO_3)_2$ at temperature of 350℃. The process of CO_2 (which is major component of inlet stream in presence of EGR) competitive adsorption dynamic changed with the ratio of CO_2 concentration and available NO_x storage sites left.

When LNT catalyst temperature varies from 150℃ to 550℃, there are new changes of NO_x storage process under different EGR rate. Nitrite route dominates at low temperature zone (150℃~200℃) because there are little NO_2 which is essential for nitrate route from NO oxidation kinetically limited at low temperature, especially near 150℃. With the increase of temperature from low temperature zone to moderate temperature zone (250℃~400℃), both of the $Ba(NO_3)_2$ and BaO-NO_2 site fraction increases significantly, especially the $Ba(NO_3)_2$ site fraction which has a 4magnitude equal to BaO-NO_2 site fraction. The cause of nitrate route participation raises first to reach same level of BaO-NO_2 site fraction and drops later is result of comprehensive effects of NO oxidation thermodynamic restriction, nitrate and nitrite thermostability and conversion between nitrites and nitrates. Nitrite route dominates again with temperature raises to high temperature zone (450℃~550℃) as a result of the reduction of nitrates formation (NO oxidation was thermodynamic limited above 350℃) and the pyrolysis of nitrates at high temperature. As EGR rate increases from 0% to 25%, both of $Ba(NO_3)_2$ and BaO-NO_2 site fraction decreases in high temperature zone which is similar with tendency of low and moderate temperature zone except for the special circumstance of $Ba(NO_3)_2$ site fraction under 0% EGR rate at 150℃ and 200℃ because oxygen atoms adsorption on Pt sites was blocked by adsorbed H_2O on Pt sites at low temperature which retarded NO oxidation resulting in reduction of nitrates produced by NO_x disproportionation (Equation 3.1 and 3.2) and reaction involving the formation of barium peroxide (Equation 3.3 and 3.4).

This work was supported by the National Natural Science Foundation of China [grant numbers 51976136, 51576140 and 51276128]; State Key Laboratory of Automotive Safety and Energy [Project No. KF1818]; National Engineering Laboratory for Mobile Source Emission Control Technology [grant numbers NELMS2019B01, NELMS2017A02]; and the Special Fund for Development of Small and Medium Enterprises [grant numbers SQ2013ZOA100012].

References

1. A. Lindholm, N.W. Currier, J. Li, A. Yezerets, L. Olsson, Detailed kinetic modeling of NOx storage and reduction with hydrogen as the reducing agent and in the presence of CO2 and H2O over a Pt/Ba/Al catalyst, J. Catal. 258 (2008) 273–288. doi:10.1016/j.jcat.2008.06.022.
2. J.R. Gonza, Applied Catalysis A : General Influence of the preparation procedure of NSR monolithic catalysts on the Pt-Ba dispersion and distribution, 363 (2009) 73–80. doi:10.1016/j.apcata.2009.04.043.

3. W.S. Epling, A. Yezerets, N.W. Currier, The effect of exothermic reactions during regeneration on the NO X trapping efficiency of a NO X storage / reduction catalyst, 110 (2006) 143–148. doi:10.1007/s10562-006-0102-2.
4. J. Ko, D. Jin, W. Jang, C. Myung, S. Kwon, S. Park, Comparative investigation of NO x emission characteristics from a Euro 6-compliant diesel passenger car over the NEDC and WLTC at various ambient temperatures, Appl. Energy. 187 (2017) 652–662. doi:10.1016/j.apenergy.2016.11.105.
5. U. Tuttlies, V. Schmeißer, G. Eigenberger, A mechanistic simulation model for NO x storage catalyst dynamics, 59 (2004) 4731–4738. doi:10.1016/j.ces.2004.08.026.
6. W.S. Epling, L.E. Campbell, A. Yezerets, N.W. Currier, J.E.P. Ii, W.S. Epling, L.E. Campbell, A. Yezerets, N.W. Currier, Overview of the Fundamental Reactions and Degradation Mechanisms of NOx Storage / Reduction Catalysts, 4940 (2007). doi:10.1081/CR-200031932.
7. S. Roy, M.S. Hegde, G. Madras, Catalysis for NO x abatement, Appl. Energy. 86 (2009) 2283–2297. doi:10.1016/j.apenergy.2009.03.022.
8. L. Lietti, M. Daturi, V. Blasin-Aubé, G. Ghiotti, F. Prinetto, P. Forzatti, Relevance of the Nitrite Route in the NOx Adsorption Mechanism over Pt-Ba/Al2O3 NOx Storage Reduction Catalysts Investigated by using Operando FTIR Spectroscopy, ChemCatChem. 4 (2012) 55–58. doi:10.1002/cctc.201100304.
9. P.F.L.L.L. Castoldi, Storage and Reduction of NO x Over LNT Catalysts, (2015) 483–504. doi:10.1007/s10562-014-1343-0.
10. S. Morandi, F. Prinetto, G. Ghiotti, L. Castoldi, L. Lietti, P. Forzatti, M. Daturi, V. Blasin-Aubé, The influence of CO2 and H2O on the storage properties of Pt-Ba/Al2O3 LNT catalyst studied by FT-IR spectroscopy and transient microreactor experiments, Catal. Today. 231 (2014) 116–124. doi:10.1016/j.cattod.2013.12.036.
11. I. Nova, L. Castoldi, L. Lietti, E. Tronconi, P. Forzatti, F. Prinetto, G. Ghiotti, NOxadsorption study over Pt-Ba/alumina catalysts: FT-IR and pulse experiments, J. Catal. 222 (2004) 377–388. doi:10.1016/j.jcat.2003.11.013.
12. L. Castoldi, R. Matarrese, S. Morandi, L. Righini, L. Lietti, Applied Catalysis B : Environmental New insights on the adsorption , thermal decomposition and reduction of NO x over Pt- and Ba-based catalysts, Appl. Catal. B Environ. 224 (2018) 249–263. doi:10.1016/j.apcatb.2017.10.019.
13. W.S. Epling, J.E. Parks, G.C. Campbell, A. Yezerets, N.W. Currier, L.E. Campbell, Further evidence of multiple NO x sorption sites on NO x storage / reduction catalysts, 96 (2004) 21–30. doi:10.1016/j.cattod.2004.05.004.
14. A. Lindholm, N.W. Currier, E. Fridell, A. Yezerets, L. Olsson, NO x storage and reduction over Pt based catalysts with hydrogen as the reducing agent Influence of H 2 O and CO 2, 75 (2007) 78–87. doi:10.1016/j.apcatb.2007.03.008.
15. X.P. Auvray, L. Olsson, Effect of Enhanced Support Acidity on the Sulfate Storage and the Activity of Pt / c -Al 2 O 3 for NO Oxidation and Propylene Oxidation, (2014) 22–31. doi:10.1007/s10562-013-1145-9.
16. Y. Ren, M.P. Harold, NO x Storage and Reduction with H 2 on Pt / Rh / BaO / CeO 2 : Effects of Rh and CeO 2 in the Absence and Presence of CO 2 and H 2 O, (2011) 969–988. doi:10.1021/cs200252r.
17. B.M. Weiss, K.B. Caldwell, E. Iglesia, NO x Interactions with Dispersed BaO : Adsorption Kinetics , Chemisorbed Species , and Effects of Oxidation Catalyst Sites, (2011) 6561–6570. doi:10.1021/jp110604j.

18. F. Sarikoc, M. Kettner, A. Velji, U. Spicher, A. Krause, A. Elsaesser, Potential of Reducing the NO X Emissions in a Spray Guided DI Gasoline Engine by Stratified Exhaust Gas Recirculation (EGR) Reprinted From : SI Combustion and Direct Injection SI Engine Technology, (2016).
19. D. Ferna, High-pressure versus low-pressure exhaust gas recirculation in a Euro 6 diesel engine with lean-NOx trap : Effectiveness to reduce NOx emissions, 20 (2019) 155–163. doi:10.1177/1468087418817447.
20. L. Liu, Z. Li, S. Liu, B. Shen, Effect of exhaust gases of Exhaust Gas Recirculation (EGR) coupling lean-burn gasoline engine on NOx purification of Lean NOx trap (LNT), Mech. Syst. Signal Process. 87 (2017) 195–213. doi:10.1016/j.ymssp.2015.12.029.
21. W.D. Chatterjee, O. Deutschmann, I.N. Feld, Detailed surface reaction mechanism in a three-way catalyst, (2001) 371–384.
22. Larson RS, Chakravarthy VK, Pihl JA, Daw CS. Microkinetic modeling of lean NOx trap chemistry. Chemical Engineering Journal. 2012;189-190:134-47.
23. F. Millo, M. Rafigh, S. Wahiduzzaman, R. Dudgeon, POLITECNICO DI TORINO Repository ISTITUZIONALE Calibration of a Global Kinetic Mechanism Based on Synthetic Gas Bench Experiments for a Lean NOx Trap Catalyst for Automotive Applications Calibration of a Global Kinetic Mechanism Based on Synthetic Gas Ben, (2017).
24. E. Fridell, H. Persson, L. Olsson, M. Skoglundh, The mechanism for NO x storage, 66 (2000) 71–74.
25. L. Lietti, M. Daturi, V. Blasin-aubø, G. Ghiotti, F. Prinetto, P. Forzatti, Relevance of the Nitrite Route in the NO x Adsorption Mechanism over Pt – Ba / Al 2 O 3 NO x Storage Reduction Catalysts Investigated by using Operando FTIR Spectroscopy, (2012) 55–58. doi:10.1002/cctc.201100304.
26. P. Koˇ, M. Marek, M. Kubíˇ, T. Maunula, M. Härkönen, Modelling of catalytic monolith converters with low- and high-temperature NO x storage compounds and differentiated washcoat, 97 (2004) 131–139. doi:10.1016/S1385-8947(03)00151-7.
27. J. Trdlic, P. Koc, M. Kubı, Transient behaviour of catalytic monolith with NO, 119 (2007) 64–72. doi:10.1016/j.cattod.2006.08.014.
28. L. Olsson, H. Persson, E. Fridell, M. Skoglundh, B. Andersson, A Kinetic Study of Oxygen Adsorption/Desorption and NO Oxidation over Pt/Al 2 O 3 Catalysts, (1999) 10433–10439. doi:10.1021/jp9918757.
29. P. Forzatti, L. Castoldi, I. Nova, L. Lietti, E. Tronconi, NO x removal catalysis under lean conditions, 117 (2006) 316–320. doi:10.1016/j.cattod.2006.05.055.
30. Liu, L., Li, Z., Liu, S. & Shen, B. Effect of exhaust gases of Exhaust Gas Recirculation (EGR) coupling lean- burn gasoline engine on NOx puri fi cation of Lean NOx trap (LNT). Mech. Syst. Signal Process. 87, 195–213 (2017).